PHYSICAL REVIEW B VOLUME 26, NUMBER 6 15 SEPTEMBER 1982

Spin-polarized electronic structure of the Ni(001) surface and thin films

O. Jepsen
NORDITA, 2100 Copenhagen, Denmark,
*and Max-Planck-Institut für Festkörperforschung, 7 Stuttgart 80, Federal Republic of Germany**

J. Madsen
Electrophysics Department, Technical University, 2800 Lyngby, Denmark

O. K. Andersen
Max-Planck-Institut für Festkörperforschung, 7 Stuttgart 80, Federal Republic of Germany
(Received 18 January 1982)

Spin-polarized energy bands, charge and spin densities have been calculated self-consistently for one, three, and five atomic (001) layers of fcc Ni using the linear augmented plane-wave method and the von Barth—Hedin approximation for exchange and correlation. The self-consistent potential of the five-layer film is used to calculate the electronic structure of a 13-layer film. The theoretical work function of 5.4 eV agrees well with the experimental value of 5.2 eV. The calculated spin moments are ordered ferromagnetically in all the films considered, and the moments of the atoms in the surface layer are 0.95, 0.69, and 0.65 Bohr magnetons for the one-, three-, and five-layer films, respectively. The moment of an atom in the central layer of the five-layer film is 0.61 Bohr magnetons as compared with the calculated (experimental) bulk value of 0.59 ± 0.01 (0.56) Bohr magnetons. The increase of the magnetic moment at the surface is mainly of $d(x^2\text{-}y^2)$ character. The calculated $4s$ contribution to the hyperfine field changes sign and becomes positive in the outermost layer. Near $k=0$, between the Fermi level and the d-band edge (which lies 0.3 eV below the Fermi level), we find no majority-spin surface states that can explain the sign reversal of the electron spin polarization near threshold. This supports the suggestion by Liebsch that, in photoemission experiments on Ni, correlation effects make the majority-spin bands appear higher in energy. With such an adjustment of our energy bands we are able to identify the two spin-up $\bar{\Sigma}$ surface bands, but not the $\bar{\Delta}_1$ band, observed in angular-resolved photoemission experiments.

I. INTRODUCTION

The development of powerful surface-sensitive experimental techniques has stimulated interest in the physical properties of crystalline surfaces and chemical processes taking place near surfaces. This progress in experimental techniques has been followed by the development of theoretical methods for calculating ground-state properties of solids with surfaces. These methods are based on band-structure techniques which have been very successful in explaining the bulk properties of nearly all elements of the Periodic Table as well as a large variety of solid compounds.

The measured and calculated properties of Ni have been a matter of some controversy. While the measured bulk magnetic moment[1] ($0.56\mu_B$) is well reproduced theoretically ($0.59\pm0.01\mu_B$),[2] angle-resolved photoemission spectroscopy (ARPS) gives a d-band width of 3.3—3.8 (Refs. 3 and 4) and an exchange splitting of 0.31—0.26 eV (Refs. 3 and 4). The calculated values are much larger, 4.5 and 0.6 eV (Ref. 2), respectively. Several explanations have been given to resolve these discrepancies. First it should be noted that the measured band narrowing is not a surface effect. A band narrowing does occur at the surface because of the reduced coordination number but, already at the second layer below the surface the bulk band width is restored and, since the sampling depth is about 10 Å, the surface layer only represents 20% of the intensity. Pendry and Hopkinson[5] have pointed out that the d-electron states far below the Fermi level have very short electron-hole lifetimes and that they therefore are suppressed in photoemission by lifetime broadening. Liebsch[6] has proposed that both the d-band narrowing and the small exchange splitting seen by ARPS can be understood on the

basis of correlation among the d-electrons, which determine the spectral distribution of the created hole. The observed symmetry dependence of the exchange splitting[3] (the t_{2g}-like X_5 level is split by 0.32 eV while the e_g-like X_2 level is split by 0.18 eV) has also been explained by Liebsch[6] as self-energy effects. He finds the splitting of the t_{2g} states to be 0.37 eV and that of the e_g states to be 0.21 eV.

Another controversy has been the position of the majority-spin d-band edge relative to the Fermi energy. Wohlfarth[7] was the first to point out that according to the simple band picture, electron emission experiments should give a negative electron-spin polarization (ESP) near threshold and then change sign for higher energies. At that time ESP measurements only showed positive polarization.[8] It was later shown by Eib and Alvarado[9] using photoemission that such a sign change does occur but only 0.05 eV above threshold, a value much smaller than the calculated binding energy of the top of the majority-spin d band (0.3 eV).[2] Kleinman and co-workers[10] proposed that this discrepancy arises from surface states above the majority-spin d bands. However, ARPS measurements show[3,4] that the majority-spin d-band edge lies less than 0.1 eV below the Fermi energy and surface states are therefore not needed to explain the ESP measurements. Furthermore, Moore and Pendry[11] have calculated the ESP in good agreement with experiments, without surface-state contributions, but with an assumed exchange splitting of 0.33 eV. This is consistent with Liebsch's[6] explanation of the apparent band narrowing and the reduced exchange splitting seen in photoemission. As a consequence of the small exchange splitting, the top of the majority-spin band is shifted towards the Fermi energy.

The third puzzle which will be particularly dealt with in this paper is the size of the magnetic moment on the Ni surface.[12] Libermann *et al.*[13] measured the magnetic moment of thin Ni films electroplated into Cu and Au substrates and, by extrapolating their data to zero temperature, they found that, independently of the thickness of the films, the two topmost layers did not possess a magnetic moment (magnetically dead). However, spin-polarized field emission from Ni(001) (Ref. 14) and ESP photoemission from Ni films condensed onto Cu (Ref. 15) seem to indicate that the surface layer is not magnetically dead, but that it has a moment of about the same size as in bulk Ni. More recently Bergmann[16] measured the magnetization of thin films of Ni condensed onto amorphous $Pb_{75}Bi_{25}$ and onto crystalline Pb, Cu, and Bi by the anomalous Hall effect. He found that films thinner than two atomic layers have no magnetic moment while thicker films do. He argued that the lack of magnetism in the thinner films may be due to the interaction between Ni and the nonmagnetic substrate and need not be a characteristic of a thin, unsupported film or a film on top of a bulk magnetic material. Finally, the variation of the magnetic moment across a nine-layer unsupported Ni film was calculated self-consistently by Wang and Freeman.[17] They found that the magnetic moment varied substantially from layer to layer and, at the surface it was 20% smaller than in the central layer.

In this paper we present *ab initio* self-consistent energy band calculations for one, three, five layers of Ni(001) films.[18] Furthermore, the self-consistent potential for the five-layer film has been used to calculate the electronic structure of a 13-layer film. The variation of the charge and spin densities through the outermost layers are found to be similar in the three-, five-, and 13-layer films. The magnetic moment is found to be somewhat larger for the surface atoms than for bulk Ni and this is in contrast with the nine-layer calculation of Wang and Freeman.[17] The surface states and resonances found in the 13-layer film are also found in the five-layer film. We clearly identify the surface states recently observed by ARPS near the $\bar{M}$ point in the Brillouin zone.[19] However, the observed surface state near $\bar{X}$ is not present in our calculation. We find a surface resonance around $\bar{\Gamma}$, 0.42 eV below the Fermi energy and with a downward dispersion away fron $\bar{\Gamma}$. This agrees well with the properties of the surface state recently observed by Erskine,[19] provided that we shift our bands upwards as a correction for the omitted correlation effects.[6]

We begin in the next section with a brief description of how the self-consistent charge densities and potentials were calculated. In Sec. III we discuss the energy bands for the different films. The surface states and resonances are identified and related to the simple energy bands for the monolayer and they are furthermore compared with angular-resolved photoemission experiments and with other calculations. The densities of states are presented in Sec. IV, where we make use of the layer-, spin-, and orbital-projected densities of states to explain the changes near the surface of the thicker films in terms of the results for the monolayer. The redistribution of charge among the d orbitals and the consequent change of aniso-

tropy of the spin density at the surface is discussed in Sec. V. At the end of that section the different attempts to measure the surface magnetic moment of Ni are discussed. Finally, the principal conclusions are summarized in Sec. VI. The potentials from which our five- and 13-layer film results may be generated can be obtained from the Physics Auxiliary Publication Service of the American Institute of Physics.[20]

II. METHOD OF CALCULATION

The energy bands and eigenvectors were calculated self-consistently using the linear augmented plane-wave (LAPW) method. The application of this method to solve Schrödinger's equation for thin films was first described in Ref. 21 and in the present section we shall merely explain how the charge density and potential used in the self-consistent calculations were constructed.

In the film geometry, illustrated in Fig. 1, space is partitioned into three regions: I, the interstitial region, II, the regions inside nonoverlapping muffin-tin (MT) spheres centered on the atoms, and III + IV, the two vacuum regions, or planar muffin tins, outside the film. In regions I, II, and III we use a set of plane waves which are Bloch waves parallel to the film and which vanish for $r_\perp = \pm A$.

An LAPW basis function is such a plane wave in region I and, in regions II and III + IV, it is constructed from the solutions of Schrödinger's equation for the appropriately symmetrized potentials: $v(\vec{r}) = V(r)$ in regions II and $v(\vec{r}) = V(r_\perp)$ in regions III + IV. Each LAPW is continuous with a continuous first derivative throughout space. Therefore, the charge density constructed from a finite sum of LAPW's is also continuous with a continuous first derivative (provided that the angular-momentum expansion inside the MT spheres is carried to convergence). For the calculation of the charge density and the potential it is convenient to express the LAPW not only in region I but also in regions II and III, i.e, throughout the A slab (see Fig. 1), as a plane wave plus the appropriate differences inside regions II and III. The electron density is then expressed as a plane-wave expansion plus a component, Δn, which vanishes in region I with a vanishing gradient along the boundaries of this region. In the self-consistent calculations we have approximated Δn by its spherical and planar averages in regions II and III, respectively. This is exact at the nuclei, at infinity, and at the MT boundaries and infinitesimally close to them. Except for systems with very localized open shells, this approximation where the non-MT part of the charge density is supplied entirely by the plane-wave expansion, is a good one.

This decomposition of the self-consistently calculated electron density for the three-layer Ni film is shown in Fig. 2 along a line perpendicular to the surface and through a nucleus in the central layer. The difference between the total density (TOT) and its plane-wave part (PW) vanishes in the interstitial region (I) and is everywhere continuous and differentiable. The decomposition of the total density

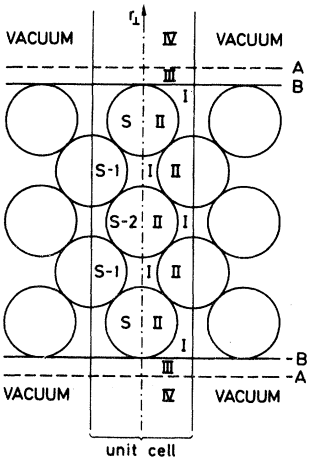

FIG. 1. Film unit cell.

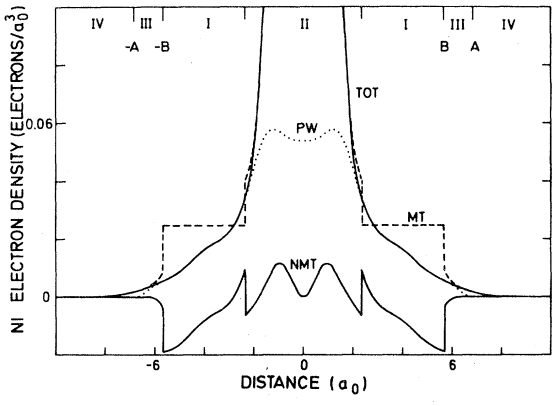

FIG. 2. Decomposition of the self-consistent electron density for the three-layer Ni film along a line perpendicular to the surface and through a nucleus in the central layer.

into MT and non-MT (NMT) parts is also shown. These parts are discontinuous at the boundaries of the interstitial region, and the non MT part vanishes in region IV.

Only the density of the valence electrons was calculated self-consistently in the film. The density of the core electrons was obtained from a self-consistent atomic calculation and added to Δn.

With the charge density expressed as a plane-wave series plus a sum of spherically or planar symmetric contributions, Δn, it is a relatively simple matter to solve Poission's equation and express the Coulomb potential in a similar way. For the the exchange-correlation potential we used the local spin-density (LSD) form, $v_{xc\sigma}(\vec{r}) = \mu_{xc\sigma}(n_\uparrow(\vec{r}), n_\downarrow(\vec{r}))$, as specified by von Barth and Hedin,[22] and we treated the nonlinear function μ_{xc} in the following, approximate way: From the MT part of the density in region II and IV we constructed

$$v_{xc\sigma}^{MT} \equiv \mu_{xc\sigma}(n_\uparrow^{MT}, n_\downarrow^{MT})$$

and in the same way we construct a term $v_{xc\sigma}^{PW}$ from the total density in regions I and III and the plane-wave part of the density in region II. The latter term was expressed as a plane-wave series in the A slap. The exchange-correlation potential now exactly equals $v_{xc\sigma}^{PW}$, in regions I and III. In region IV we used the MT approximation, $v_{xc\sigma}^{MT}$, and in region II we used the approximation $v_{xc\sigma}^{MT} + v_{xc\sigma}^{PW} - [v_{xc\sigma}^{PW}]_{MT}$, where the square brackets indicate the spherical average. In region II we thus treated the large MT part of the exchange-correlation potential exactly while the small non-MT part was exact only at, and infinitesimally inside, the spheres.

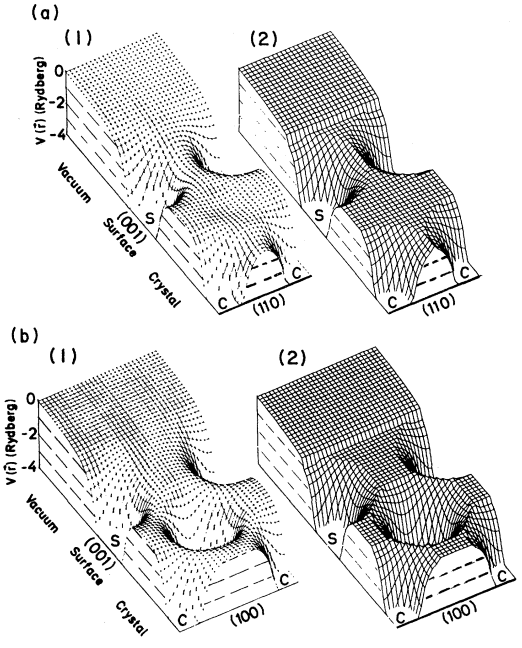

FIG. 3. Variation of the majority-spin potential in (a) a (110) and (b) a (100) plane perpendicular to the film and containing the surface atom (S), the subsurface atom and the central atom (C) for five-layer Ni(001) film. Part (1) is the full self-consistent potential and part (2) is its muffin-tin average.

The resulting self-consistent potential is illustrated in Figs. 3(a)(1), 3(b)(1), and 4. In Figs. 3(a)(2) and 3(b)(2), we show its MT-average which is spherically symmetric inside the spherical tins, planar symmetric in the planar tins outside the B slab and constant between the tins. The MT part was only used for the construction of the LAPW basis functions and in our one-electron Hamiltonian matrix the non-MT part of the potential was included as plane-wave matrix elements throughout the A slab. Outside the A slab we neglected the variation of the potential parallel to the film. The potential is listed in Ref. 20.

All integrations over the two-dimensional Brillouin zone (2D BZ) were performed by the linear triangular method[21] with 36 k points in the irreducible part of the zone (Fig. 5). The charge density was found to converge within 30—50 iterations and with the use of only 15 k points. The spin densities, however, were very unstable and several hundred iterations with the 36-point mesh were needed to obtain the converged solution. In the present calculations more than 45 LAPW's per atom were included. This resulted in mRy accuracy.

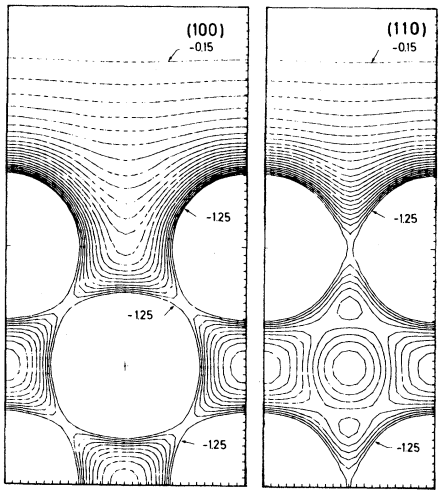

FIG. 4. Contour map of the majority-spin potential in a (100) and (110) plane perpendicular to the film for five-layer Ni(001) film. The signatures are in Rydberg units and the step is 0.05 Ry.

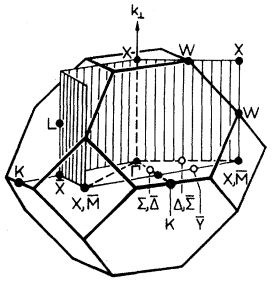

FIG. 5. Projection of the bulk fcc Brillouin zone onto the (001) two-dimensional surface Brillouin zone.

The bulk Ni lattice constant ($a = 6.659$ Bohr radii) was used for all the films. No surface reconstruction occurs for Ni(001),[23] but an outwards relaxation of the surface layer by 2.5% has been suggested by low-energy electron diffraction (LEED) analysis.[24] In our calculations such an expansion was neglected.

The relativistic effects, except the spin-orbit coupling, were included in the calculations. This was achieved through the use of a scalar-modified radial Dirac equation.

III. SURFACE STATES AND RESONANCES

In this section we present our energy bands calculated for one, five, and 13 (001) layers of Ni. From these results the surface states and resonances for a semi-infinite Ni crystal are deduced and compared with results of angle-resolved photoemission experiments. It turns out that all surface states and resonances for the semi-infinite crystal are present among the energy bands of the monolayer. Moreover, our discussions of the orbital-projected densities of states at the surface in Sec. IV and of the anisotropy of the spin density at the surface in Sec. V are based on a thorough understanding of the results for the monolayer. We therefore start by presenting these results and interpret them using simple tight-binding theory.

A. Energy bands for an (001) monolayer of Ni

The self-consistent LAPW energy bands for spin-up (majority) and spin-down (minority) electrons are shown in Fig. 6 along the lines of high symmetry in the two-dimensional Brillouin zone (Fig. 5) of the square lattice. The irreducible representation 1 (2) is even (odd) with respect to the mirror plane which contains the symmtry line in question and is perpendicular to the surface. The two bands $\bar{\Gamma}_5$-($\bar{\Delta}_2$,$\bar{\Delta}_1$)-($\bar{X}_3$,$\bar{X}_4$)-($\bar{Y}_1$,$\bar{Y}_2$)-$\bar{M}_5$-($\bar{\Sigma}_2$,$\bar{\Sigma}_1$)-$\bar{\Gamma}_5$ are odd with respect to the mirror plane in the center of the film while all other bands shown are even. (Throughout the present paper even-odd refers to this latter symmetry while the parity with respect to a mirror plane perpendicular to the surface is being referred to as 1-2.) This band structure, consisting of five narrow *d* bands which are crossed by and hybridize with a broad *sp* band, is similar to those previously obtained for (001) monolayers of Cu (Ref. 25) and Pd.[26]

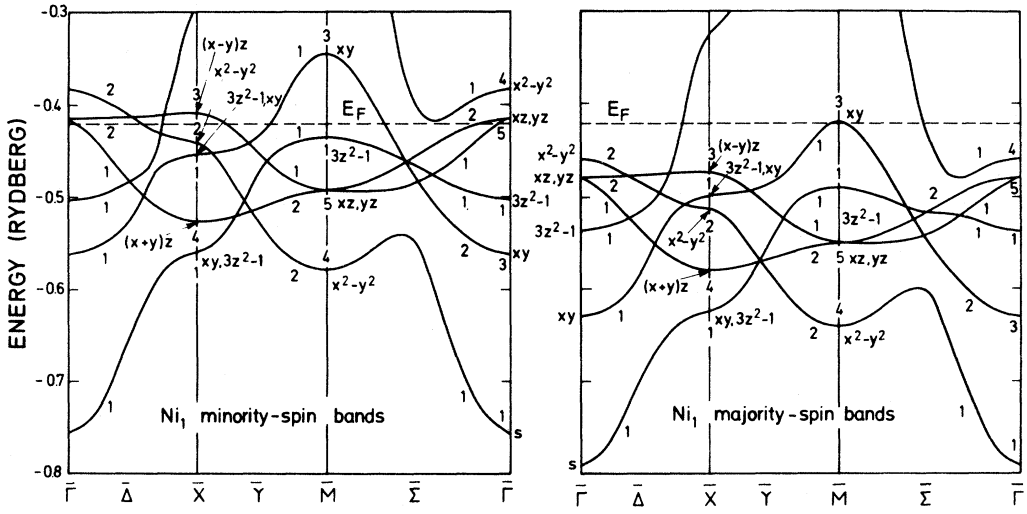

FIG. 6. Self-consistent majority- and minority-spin bands for the Ni(001) monolayer. The orbitals refer to the cubic axes in the bulk.

The widths and dispersions of the five d bands may be understood from tight-binding theory. For the two-center integrals we shall use the canonical values[27]

$$dd(\sigma,\pi,\delta)=(-6,4,-1)(R_1/R)^5\Delta\ , \tag{3.1}$$

where R is the interatomic distance and $R_1=a/\sqrt{2}$ is the distance to the first-nearest neighbor. For the width parameter we take the nonmagnetic bulk value (in units of mRy)

$$\Delta=10(s/R_1)^5(\mu s^2)^{-1}=5.9\ , \tag{3.2}$$

where $s=a(3/16\pi)^{1/3}$ is the Wigner-Seitz radius, a is the bulk lattice constant, and $\mu=13$ is the self-consistent bulk d band mass.[28,2] With this tight-binding model including first- and second-nearest-neighbor interactions, i.e., $R_1/R=1$ and $1/\sqrt{2}$, respectively, the following results are easily obtained.

The two odd bands, degenerate at $\bar{\Gamma}_5$ and $\bar{M}_5$, which do not hybridize with any of the other bands, have xz and yz character. Here, and in the following, x, y, and z refer to the bulk cubic directions with z perpendicular to the film and x and y in the $\bar{\Sigma}$ directions in Fig. 5. The dispersion of the (xz,yz) bands, in units of Δ, is

$$3(i+j)+6(2)^{-5/2}ij\pm5[(i-j)^2+2^{-3}(i'j')^2]^{1/2}\ , \tag{3.3}$$

where $i\equiv\cos(k_ia/\sqrt{2})$ and $i'\equiv\sin(k_ia/\sqrt{2})$. Here, i and j refer to the directions of the primitive translation vectors of the square lattice, i.e., to the $\bar{\Delta}$ directions in Fig. 5. The terms linear in i and j are due to interactions between first-nearest neighbors, and the quadratic terms are due to interactions between second-nearest neighbors. The latter terms are small and in Fig. 6 their effect is most clearly seen as the splitting between the $\bar{\Sigma}_1$ and $\bar{\Sigma}_2$ bands. The energies at the points of high symmetry ($\bar{\Gamma}$: $i=j=1$, $\bar{X}$: $i=-j=1$, $\bar{M}$: $i=j=-1$) as well as the largest bandwidth reached at $\bar{X}$, are given in Table I. The agreement with the full LAPW calculation in Fig. 6 is better than 15 mRy.

The $\bar{\Gamma}_3$-$\bar{\Delta}_1$-$\bar{X}_1$-$\bar{Y}_1$-$\bar{M}_3$-$\bar{\Sigma}_2$ band has purely xy character in $\bar{\Gamma}$, along $\bar{\Sigma}$, and in $\bar{M}$ but, along $\bar{Y}$ and $\bar{\Delta}$, it hybridizes with the $3z^2-1$ and the sp bands. Neglecting this hybridization the dispersion of the xy band is

$$-\tfrac{19}{2}(i+j)+16(2)^{-5/2}ij \tag{3.4}$$

TABLE I. Tight-binding d band for a square lattice. The first term arises from interactions between nearest neighbors and the second from interactions between next-nearest neighbors.

E/Δ	$\bar{\Gamma}$	$\bar{X}$	$\bar{M}$	Width
xz,yz	$6+1.1$	$\pm10-1.1$	$-6+1.1$	20
xy	$-19+2.8$		$19+2.8$	38
		$\pm8.9-0.6$		
$3z^2-1$	$-9-1.6$		$9-1.6$	18
x^2-y^2	$16-3.4$	$0+3.4$	$-16-3.4$	32

such that the bandwidth is 38, with the bottom at $\bar{\Gamma}$ and the top at $\bar{M}$. We shall see later that the $\bar{M}_3$ state will develop into a surface state lying above the top of the d-band continuum for the semi-infinite crystal. In the tight-binding approximation, with identical parameters for the bulk and the monolayer, the energy of the top of the d-band continumm at $\bar{M}$, the X_5 bulk state (Figs. 5 and 7), equals that of the $\bar{M}_3$ state for the monolayer because, in the bulk, the interactions beteen the xy orbital and its four first-nearest neighbors in the $z=a/2$ plane cancel, and so do the interactions with those in the $z=-a/2$ plane. Only the $dd\delta$ interactions with the two second-nearest neighbors in the $z=\pm a$ planes make the bulk level lie slightly below the film level.

The $3z^2-1$ band starts off at $\bar{\Gamma}_1$ and $\bar{M}_1$ where it hybridizes with the s band. Along the high-symmetry lines and at $\bar{X}$ it furthermore hybridizes with the xy band. Neglecting this hybridization, the dispersion of the $3z^2-1$ band is

$$-\tfrac{9}{2}(i+j)-9(2)^{-5/2}ij\ , \tag{3.5}$$

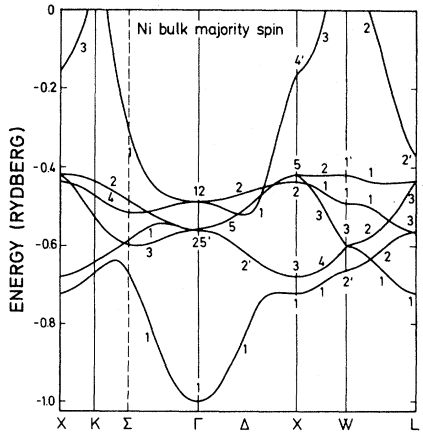

FIG. 7. The majority-spin bulk bands of Ni as calculated from the muffin-tin potential in the central layer of the five-layer Ni film.

such that the bandwidth is no more than 18, the bottom being at $\bar{\Gamma}$ and the top at $\bar{M}$. The matrix element for hybridization between the xy and $3z^2-1$ bands is

$$(5\sqrt{3}/2)(i-j)\ . \tag{3.6}$$

The separation between the $\bar{X}_1$ levels thus becomes 17.8×5.9 mRy, and this is in good agreement with the result of the full calculation shown in Fig. 6. By comparison with the center of gravity for the purely d-like $\bar{X}_3$ and $\bar{X}_4$ levels, it may be seen that the hybridization with the above-lying sp band pushes the $\bar{X}_1$ levels down in energy by approximately 25 mRy for the spin-up bands and 40 mRy for the spin-down bands.

The $\bar{\Gamma}_4$-$\bar{\Delta}_2$-$\bar{X}_2$-$\bar{Y}_2$-$\bar{M}_4$-$\bar{\Sigma}_1$ band has pure x^2-y^2 character, except along $\bar{\Sigma}$, where it hybridizes with the $3z^2-1$ and sp bands. Neglecting this hybridization, the dispersion of the x^2-y^2 band is

$$8(i+j)-19(2)^{-5/2}ij \tag{3.7}$$

such that the maximum is reached at $\bar{\Gamma}$ and the minimum at $\bar{M}$. The corresponding values are given in Table I. We shall later see that the x^2-y^2 band near $\bar{\Gamma}$, which, next to the xy band near $\bar{M}$, is the level of highest energy, develops into a surface resonance lying slightly below the top of the bulk d band. In the tight-binding approximation the energy of the bulk X_2 state (Fig. 7) is higher than that of the film $\bar{\Gamma}_4$ state by the amount 5.5Δ. This difference is due to the interaction between the x^2-y^2 orbital and its eight first-nearest neighbors in the planes $z=\pm a/2$.

Not only the number of nearest neighbors, and hence the off-diagonal elements of the canonical tight-binding Hamiltonian, differs between a monolayer and a crystal but also the diagonal elements, the orbital energies, might differ. In the Ni crystal the difference between the energies of the $e_g(3z^2-1,x^2-y^2)$ and the $t_{2g}(yz,xz,xy)$ orbitals is negligible and, for the Ni monolayer, we find by comparison of the tight-binding results given above with the LAPW results in Fig. 6 that the orbital energies differ by less than 15 mRy. This difference is rather small and in the surface layer of a semi-infinite crystal the orbital energies would differ by even less.

It is possible to improve the tight-binding fit to the LAPW calculation for the monolayer by using for the width parameter Δ the values 5.5 and 5.9 mRy for spin-up and spin-down, respectively. The fact that the majority-spin band is more narrow than the minority-spin band is due to the energy dependence of the effective LSD Stoner exchange parameter, which leads to a larger exchange-splitting at the top than at the bottom of the d band.[29] This difference in spin-up and spin-down bandwidths is proportional to the magnetization and it is therefore smaller in the bulk ($\Delta=5.8$ and 6.1 mRy), where the spin magnetization is $0.58\mu_B$/atom, than in the monolayer where the spin magnetization is $0.95\mu_B$/atom. We shall return to the magnetization results in Sec. V.

B. Energy bands for five and 13 (001) layers of Ni

The self-consistent LAPW energy bands for the spin-up electrons in the five-layer film (Ni_5) are shown in Fig. 8. The spin-down bands close to the Fermi level are shown in Fig. 9 and apart from a shift, the exchange-splitting, they are quite similar to the spin-up bands.

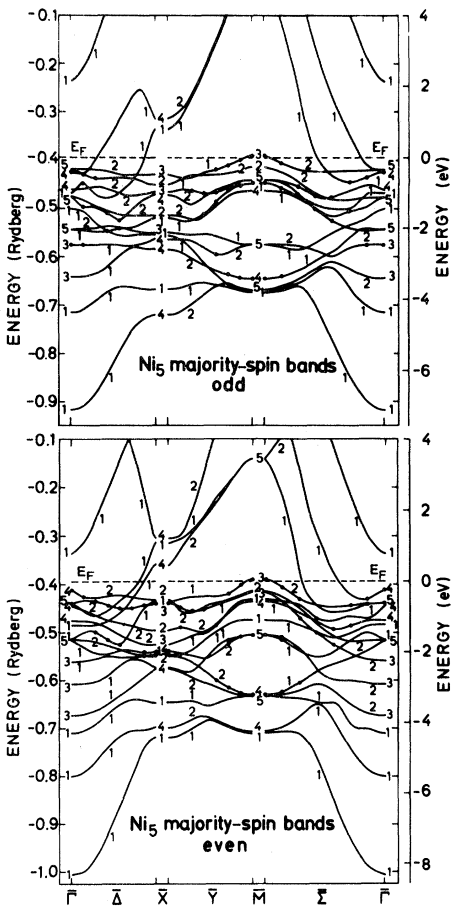

FIG. 8. Even and odd majority-spin bands for the five-layer Ni(001) film.

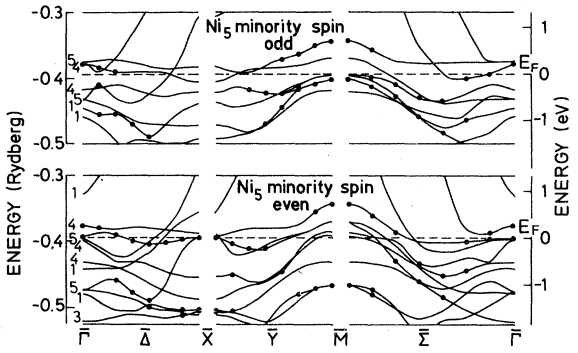

FIG. 9. Minority-spin bands for the five-layer Ni(001) film.

The labels even and odd refer to the parity with respect to the mirror plane lying in the center of the film. Most of the states behave like standing waves in the direction perpendicular to the film, that is, like $\cos(r_\perp k_\perp^e)$ with $k_\perp^e \approx (n+1/2)\pi/A$ for the even states, and like $\sin(r_\perp k_\perp^o)$, with $k_\perp^o \approx n\pi/A$ for the odd states. For an infinitely thick film ($A \rightarrow \infty$) these even and odd states would be degenerate and could form the Bloch states, $\exp(\pm i r_\perp k_\perp)$. The remainder of the states would develop into surface states and resonances. Although the states for a film of finite thickness cannot exactly be separated into bulk (Bloch) states, surface states, and surface resonances, we have tried to do so.

Experimentally the question of how thick films are needed for d-like surface states and resonances to be observed was considered by Weng and El-Batanouny.[30] These authors studied the photoemission from thin Pd(111) films evaporated onto the (110) face of recrystallized Nb foils. Pd(111) surface states could be identified when the third atomic layer began to pile up and, by the time four layers were completed, the surface states were fully established and the photoemission energy-distribution spectrum was similar to that of the (111) face of a Pd single crystal.

We therefore felt justified in using our five-layer calculation for Ni in the search for surface states, and we first sorted out the states with more than 60% of the charge inside the two muffin-tin spheres, on either side of the film, and which seemed to decay towards the center of the film. These states are indicated in Fig. 8 and 9 by black dots at the calculated $\vec{k}$ points but, due to the oscillatory behavior of the charge density for standing-wave bulk states together with the small width of the film, they may include prospective bulk states. Moreover, slowly decaying surface states or resonances may have escaped the sorting. Only in those cases where the states appear as even-odd pairs, split considerably less than the neighboring (in $\vec{k}_{||}$ and E) delocalized states, have prospective surface states or resonances been identified. As may be seen in Figs. 8 and 9 this happened in many but certainly not in all cases.

As a consequence we felt it was necessary to perform calculations for a 13-layer-thick film and this finally enabled us to sort out the surface states and resonances as degenerate even-odd pairs. The results for both directions of spin are shown in Fig. 10 and they will be discussed below.

The 13-layer calculation was not self-consistent and it employed a muffin-tin potential. This was generated from the muffin-tin part of the self-consistent five-layer potential in the following way: The potential in the vacuum and in the two outermost muffin-tin spheres of the 13-layer film was as in the five-layer film and, in the remaining nine inner spheres, the potential from the central sphere was used. The muffin-tin constant, extending through the interstitial region (I in Fig. 1) from $-B$ and B, was equal to that of the five-layer film. By comparing the results of the 13-layer muffin-tin calculation (Fig. 10) with those of the five-layer self-consistent non-muffin-tin calculation (dots in Figs. 8 and 9) and, furthermore, with those of a five-layer calculation employing only the muffin-tin part of the potential, we found the results shown in Fig. 10 to be reliable, despite the crudeness of the potential. The muffin-tin as well as the non-muffin-tin parts of the self-consistent, spin-polarized five-layer potential are tabulated in Ref. 20.

In Fig. 10 we have distinguished between surface states, indicated by full lines, and surface resonances, indicated by dotted lines. The former lie

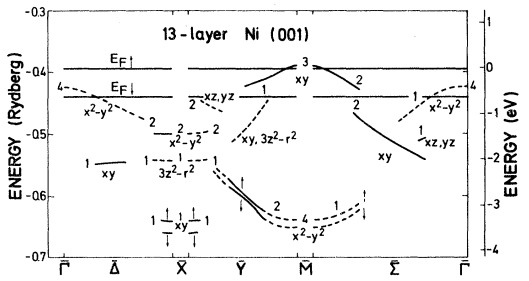

FIG. 10. Surface states (full line) and surface resonances (dotted line) for the 13-layer Ni(001) film. The energy scale refers to the spin-up bands and Fermi level. The spin-down bands and Fermi level have been shifted downwards such that the two band structures coincide near the Fermi level.

in gaps (between states of the same surface symmetry) of the bulk band structure projected onto the two-dimensional Brillouin zone, while the latter do not. The projection of the three-dimensional Brillouin zone onto the two-dimensional Brillouin zone was illustrated in Fig. 5, the majority-spin bulk band structure was shown in Fig. 7, and its two-dimensional projection is shown in Fig. 11.

The bulk band structure was calculated with the bulk LAPW method using the muffin-tin part of the potential in the central sphere of the five-layer film and the same muffin-tin constant. Our bulk band structure agrees with that of Wang and Callaway[2] for the same exchange-correlation approximation to about 10 mRy for the *d* bands and about 40 mRy for the *sp* bands. The differences are mainly caused by the fact that our muffin-tin constant is higher than what a bulk calculation would have given because, in the film, the potential increases towards the surfaces. Therefore, the discrepancies are larger for the more diffuse *sp* like levels than for *d*-like levels. For our purpose of distinguishing between surface states and resonances for the 13-layer calculation, it is appropriate to use the "same" muffin-tin potential in bulk and film calculations.

Both spin-up and spin-down surface bands are shown in Fig. 10 but the spin-down bands have been shifted downwards in energy by the exchange splitting of 0.61 eV such that they coincide with the spin-up bands near the Fermi level. Plotted in this way only the states far away from the Fermi level, towards the bottom of the *d* band, do not coincide due to the slightly different widths of the spin-up and spin-down bands mentioned in the preceding section. This means that we have found no surface states to exist for only one of the spin directions and that, in the LSD approximation, the exchange splitting depends only on energy and not on the symmetry of the state.

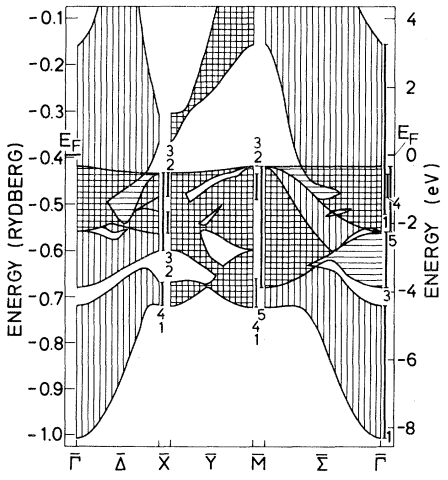

FIG. 11. Majority-spin Ni bulk bands projected onto the two-dimensional Brillouin zone. Vertical and horizontal shadings refer to bands of symmetry 1 and 2, respectively.

From the LAPW wave functions we have projected out the partial-wave characters. For each surface band the dominating character has been indicated in Fig. 10 and the close relation with the electronic structure of the monolayer shown in Fig. 6 and analyzed in the preceding section is obvious. We believe that these findings are independent of the muffin-tin approximation used in the 13-layer calculation because they are consistent with the results of the five-layer calculation performed without this approximation.

C. Comparison with angular-resolved photoemission experiments

It is interesting to compare our calculated surface states with those found in recent angular-resolved photoemission experiments (ARPS) by Plummer and Eberhardt and by Erskine.[19] The criteria used by these authors for assigning a peak in a measured energy distribution curve to an occupied surface state were (i) that the peak should attenuate with surface contamination, (ii) it should show no dispersion with the momentum perpendicular to the surface, and (iii) it should lie in a gap in the symmetry and spin-projected bulk band structure. The third condition was furthermore used to identify the spin direction of a surface state and Erskine, in addition, identified the surface-state symmetry in this way. A surface state was distinguished from a surface resonance by the narrowness of the peak, which should be comparable to that of known transition-metal surface states of similar binding energy. It should, however, be noted that little is known about the width of surface *resonances* with small binding energies.

Plummer and Eberhardt found two surface bands: (1) a $\bar{\Sigma}_2$ band running from $\bar{M}$ and halfway towards $\bar{\Gamma}$, and (2) a $\bar{\Delta}_1$ band running from $\bar{X}$ and one-third the way towards $\bar{\Gamma}$. Both bands were less than 0.1 eV below the Fermi level and had nearly no dispersion. From condition (iii) mentioned above the $\bar{\Sigma}_2$ band was assigned to the spin-up bands while the $\bar{\Delta}_1$ band was assigned to the spin-down band.

The $\bar{\Sigma}_2$ spin-up surface state may be identified in

our calculation: It has predominantly xy character, extends through a region of k space around $\bar{M}$ and becomes unoccupied close to the $\bar{M}$ point. This $\bar{\Sigma}_2$ state has more than 90% of the charge on the two surface atoms on either side of the film. For the state $\frac{6}{7}\,\bar{\Gamma}\,\bar{M}$ this is illustrated in Fig. 12 which shows contours of constant electron density in the (110) plane perpendicular to the surface. The probability density on nonsurface atoms is less than 0.07 electrons a_0^{-3}.

The alleged spin-down $\bar{\Delta}_1$ surface band close to the Fermi level cannot be identified in our calculation: The $\bar{\Delta}_1$ spin-down surface resonance of $3z^2-1$ character seen in Fig. 10 is lying as much as 1.5 eV below the Fermi level.

Erskine reported a surface band with 0.11 eV binding energy at $\bar{\Gamma}$. The band dispersed downwards from $\bar{\Gamma}$ along the $\bar{\Sigma}$ line and at two-thirds the way to $\bar{M}$ it reached a binging energy of 0.14 eV. This surface band was assigned to spin-up surface *states* of $\bar{\Sigma}_2$ symmetry because only for this symmetry and spin direction is there a gap below the Fermi level in the projected bulk bands (the experiment was conducted with unpolarized light and he could therefore not distinguish between $\bar{\Sigma}_1$ and Σ_2 initial states). From our band structure we, however, conclude that the observed band is the spin-up surface *resonance* of predominantly x^2-y^2 character and therefore of $\bar{\Sigma}_1$ symmetry.

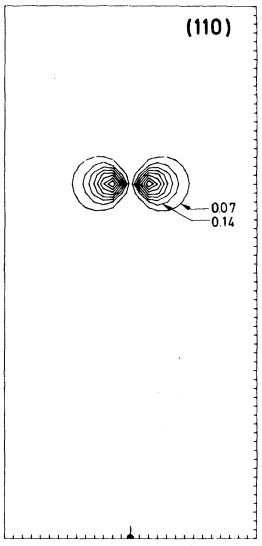

FIG. 12. $\bar{\Sigma}_2(xy)$ surface state at $\frac{6}{7}\bar{\Gamma}\bar{M}$: Contours of constant probability density (in units of a_0^{-3}) in the (110) plane perpendicular to the surface. (The x, y, and z axes are oriented along the cubic axes in the bulk.) The positions of the neighboring atoms are indicated by dots. Density step equals $0.07a_0^{-3}$.

Compared with experiment, our calculated spin-up xy surface state and our calculated spin-up x^2-y^2 surface resonance have too large binding energies and too strong dispersions. These discrepancies may presumably be accounted for by the correlation effects neglected in our calculations: Liebsch[6] estimated that the binding energies of the calculated t_{2g} states (xy, xz, and yz) near the Fermi level should be reduced by the factor 0.62 and that the binding energies of the calculated e_g states (x^2-y^2 and $3z^2-1$) should be reduced by 0.35. These corrections would thus reduce the calculated value of the exchange splitting from 0.61 to 0.37 eV for the t_{2g} states and to 0.21 eV for the e_g states. That the estimates made for the bulk Ni are approximately valid for Ni surfaces too, may be inferred from the 0.30 eV exchange splitting recently measured[31] for mixed t_{2g} and e_g surface states on Ni(110). By taking the correlation corrections into account, the binding energy of our $\bar{\Sigma}_2$ xy spin-up surface state at $\frac{1}{3}\bar{M}\,\bar{\Gamma}$ is 0.27 eV, and the binding energy of the $\bar{\Gamma}_4$ x^2-y^2 spin-up surface resonance is 0.15 eV.

D. Comparison with other calculations

The general features of our bands are similar to those obtained with the nine-layer, self-consistent, spin-polarized linear combination of atomic orbitals (LCAO) method by Wang and Freeman,[17] with the 35-layer, spin-polarized, parametrized LCAO method by Dempsey and Kleinman[10] and with the nine-layer, self-consistent LCAO method by Arlinghouse *et al.*[32] Apart from the xy surface state around $\bar{M}$, which occurs in all calculations, there are, however differences between the surface bands obtained in the various calculations. We shall only comment on the controversial surface bands near $\bar{\Gamma}$ and close to the Fermi energy.

Kleinman and collaborators found a weak spin-up $\bar{\Gamma}_5$-$\bar{\Sigma}_2$-$\bar{M}_2$-$\bar{Y}_2$-$\bar{X}_2$-$\bar{\Delta}_2$ surface state and a weak $\bar{\Sigma}_1$-$\bar{\Gamma}_5$-$\bar{\Delta}_1$ surface resonance with 0.08 eV binding energy near $\bar{\Gamma}$. These states were held responsible for the measured sign reversal of the photoelectron spin polarization near threshold. The calculated sign change occurred at 0.12 eV above threshold. In addition they found a strong $\bar{\Sigma}_1$-$\bar{\Gamma}_4$-$\bar{\Delta}_2$ surface resonance with 0.18 eV binding energy near $\bar{\Gamma}$. This resonance contributed to the positive spin polarization above the energy where the sign change occurred. Wang and Freeman found a very weak $\bar{\Gamma}_5$ and a strong $\bar{\Gamma}_4$ surface state, but the binding energies were 0.24 and 0.33 eV, respectively, and

none of these states extended away from the $\bar{\Gamma}$ point. We do not find any occupied spin-up surface states above the top of the d-band continuum at $\bar{\Gamma}$. Our $\bar{\Gamma}_5$ state lies in the continuum, it has a binding energy of 0.34 eV and it can, at most, be characterized as a very weak surface resonance. Our spin-up $\bar{\Gamma}_4$ x^2-y^2 surface resonance at 0.42-eV binding energy has 72, 20, and 5% of its density in, respectively, the first, the second, and the third layer below the surface. This state is shown in Fig. 13.

IV. DENSITIES OF STATES

In this section we present the densities of states for one, three, and five (001) layers of Ni. We shall see that in all cases it is essentially only the local density of states at the surface layer that differs from the density of states in the bulk. Moreover, the difference is similar for the three- and five-layer films, and this indicates that the spin density at the surface of a five-layer film closely resembles that of a semi-infinite crystal. The difference between the surface and bulk projected densities of states will be discussed on the basis of the tight-binding analysis of the monolayer and bulk states given in Sec. III A.

In Fig. 14 we show the layer and orbital projected densities of states for the monolayer and for the center and surface layers of the five-layer film. The structures for the two spin directions are seen to be nearly identical and we can therefore restrict our discussion to one spin direction.

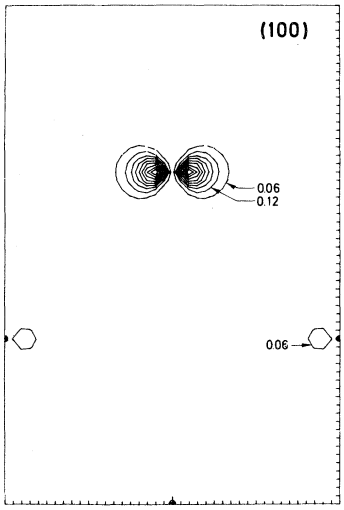

FIG. 13. $\bar{\Gamma}_4(x^2-y^2)$ surface state: contours of constant probability density in the (100) plane perpendicular to the surface. Density step equals $0.06a_0^{-3}$.

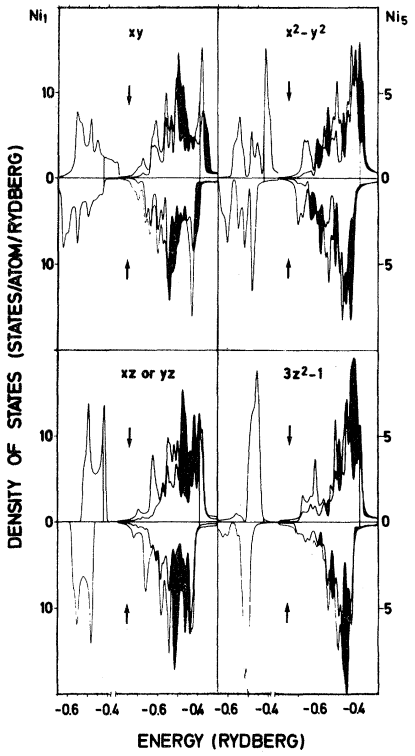

FIG. 14. Layer- and orbital-projected densities of states. To the left in each box is shown the result for the one-layer film and to the right are shown the results for the central and the surface layer of the five-layer film. The shaded areas indicate excess states on the surface. The Fermi energy is indicated by a vertical line.

The layer and orbital projected densities of states and charges presented in this and the following sections refer to the partial waves in the muffin-tin spheres. The densities of states shown in Figs. 14–19 we smoothed with a Gaussian of width 10 mRy.

In the nearest-neighbor tight-binding model for the monolayer described in Sec. III A the densities of states of the unhybridized xy, x^2-y^2, and $3z^2-1$ bands [Eqs. (3.4), (5), and (7)] have the same shape. This shape consists of a peak at the center of the band, which is approximately the same for all three orbitals, and steps at the top and bottom of the band. Only the $3z^2-1$ band approximately preserves this shape when hybridization and interactions with more distant neighbors are taken into account. The $3z^2-1$ band is approximately half as wide as the xy and x^2-y^2 bands, because the $3z^2-1$ orbital points perpendicular to

the layer while the xy and x^2-y^2 orbitals lie in the layer.

The hybridization of the monolayer x^2-y^2 band with the sp and $3z^2-1$ band causes two hybridization gaps and hence the three-peak structure seen in Fig. 14. The main peak at the top of the band is empty for the down spins and full for the up spins and contributes to the large magnetic moment ($0.95\mu_B$ per atom) of the monolayer. This peak is also found in the surface and bulk projected densities of states but it has a higher energy for the surface where it arises from the x^2-y^2 resonance. The peak in the surface density of states is half full for the down spins and full for the up spins while the peak for the bulk is occupied for both spins. Therefore some increase in the surface magnetic moment of x^2-y^2 character is to be expected.

The $3z^2-1$ projected density of states for the monolayer consists of a narrow peak which is also clearly recognized in the surface projection for the five-layer film. The peak is nearly occupied for both directions of spin and therefore does not appreciably change the surface magnetic moment.

The width of the xy density of states for the monolayer is comparable to that of the xy projected density of states for the surface layer and to that of the t_{2g} projected density of states in the bulk. This is so because the lobes of the xy orbital points towards the nearest neighbors in the plane of the layer. The structure is, however, quite different. The characteristic peak of t_{2g} character at the top of the bulk d band (see the central layer xy, xz, or yz projections in Fig. 14) is missing in the monolayer because the peak originates from interactions between layers parallel to the plane of the xy lobes. The surface layer shows a reminiscense of the peak due to the presence of half the neighboring (001) layers. The peak of the surface layer is smaller and broader than the corresponding peak from the central layer, and this broadening gives rise to the surface states near $\bar{M}$ discussed in the preceding section. Moreover, the broadening gives rise to an increased xy character of the magnetic moment near the surface.

The xz and yz orbitals are perpendicular to the (001) layers. For the monolayer the narrow, doubly degenerate xz,yz band [Eq. (3.3)] does not hybridize with other d bands and its state density consists of two peaks. The lower-lying peak arises from a region in k space around the $\bar{Y}$ line and the high-lying from a region around the $\bar{\Delta}$ line. The narrow double-peak structure may be recognized in the surface projected density of states for the five-layer film too, although it is somewhat changed and broadened, in particular on the low-energy site, due to interactions with the adjacent layers. In the bulk the high-lying peak develops into the t_{2g} peak at the top of the d band. This peak lies above the peak for the surface layer, and the xz, yz character of the magnetic moment is therefore larger in the bulk than at the surface.

In Fig. 15 we show the layer- and orbital-projected densities of states for the center and surface layer of the three-layer film. The *changes* at the surface are seen to be similar to those for the five-layer film. When all the orbital projected densities of states, including sp projections, are added we obtain the layer-projected densities of states. The projections for the central and surface layers are compared in Figs. 16(a) and 16(b) for the three-layer film and for the five-layer film. The similarity of the results for the two films is obvious. By comparison with Figs. 14 and 15 we can determine the orbital character of the excess states in the surface layer. The weak shoulder at the d-band edge for the surface layer is due to the surface states of xy character around $\bar{M}$, and in the highest-lying d-band peak the excess of states in the surface layer has x^2-y^2 character. The main

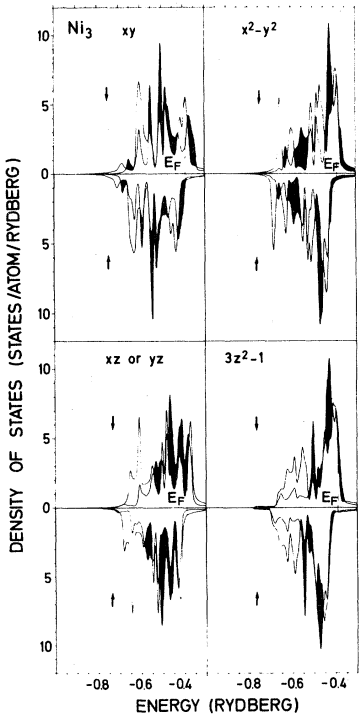

FIG. 15. Layer- and orbital-projected densities of states for the surface and the central layer of the three-layer film. The shaded areas indicate excess states on the surface layer.

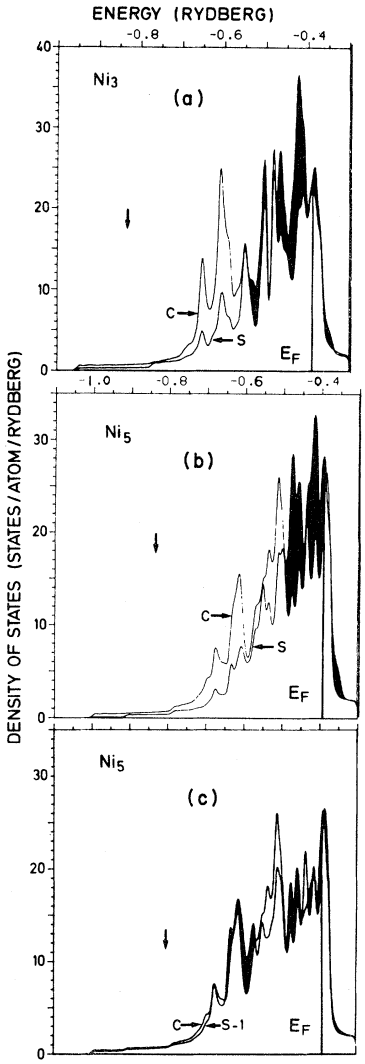

FIG. 16. Minority-spin local densities of states (a): for the surface and the central layer of the three-layer film, (b): for the surface and the central layer of the five-layer film, and (c): for the subsurface and the central layer of the five-layer film. The shaded areas indicate excess states on the outermost layer.

increase in the surface density of states occurs below the Fermi level and for the spin-down bands in the energy region between -0.4 to -0.5 Ry where all d orbitals contribute.

A demonstration that only the electronic states at the surface layer are changed significantly is given in Fig. 16(c) which shows that the densities of states change little when going from the central to the subsurface layer of a five-layer film.

Finally we show the total densities of states for one, three, and five layers of Ni(001) in Figs. 17, 18, and 19, respectively. As the film thickness decreases there is a clear narrowing and shift of weight to higher energies. It is obvious that only the local density of states for the central layer (Fig.

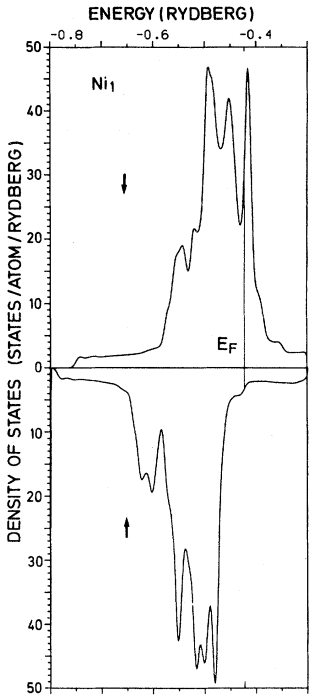

FIG. 17. Total density of states for the one-layer film.

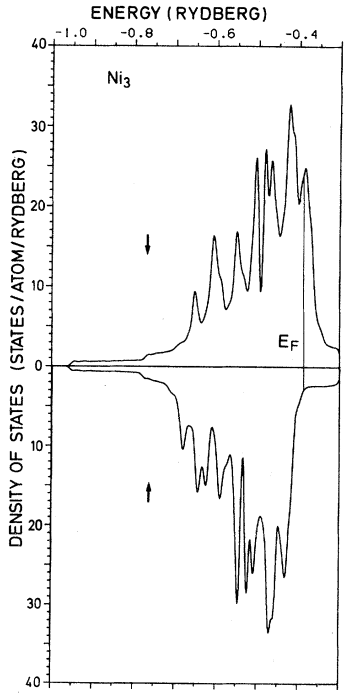

FIG. 18. Total density of states for the three-layer film.

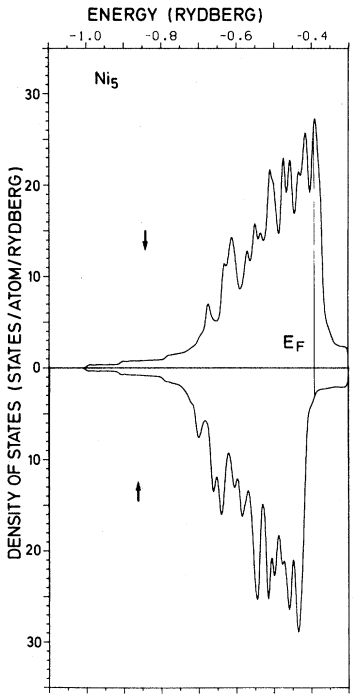

FIG. 19. Total density of states for the five-layer film.

16) and not the total density of states for the three- and five-layer films, closely resemble the density of states for the infinite Ni crystal.

V. ELECTRON AND SPIN DENSITIES

In this section we present and discuss the electron and spin densities calculated for the one-, three-, and five-layer films.

A. Electron densities

The layer and orbital projected (or more accurately, muffin-tin and partial-wave projected) valence charges are listed in Table II. Here, S, $S-1$, etc. refer to, respectively, the layer at the surface, the subsurface layer, and so on. The first two columns show that the surface charge of sp character is reduced compared with the bulk charge by 0.16 electrons for the three- and five-layer films and about twice as much for the monolayer and that the total d-orbital charge is closely the same for all layers and independent of film thickness. The charge missing inside the spheres (region II in Fig. 1) is found in the interstitial (I) and vacuum regions (III and IV). For a nonsurface layer the interstitial charge is about 0.7 electrons and for the surface layer, where the interstitial region is larger, it is somewhat increased. Independently of the film thickness we find 0.13 electrons in each of the vacuum regions.

Whereas the total d charge is the same for all atoms, there is a redistribution of charge among the five d orbitals in the surface layer. Below the surface layer the three t_{2g} orbitals (xy,xz,yz) are nearly equally populated and so are the two e_g orbitals (x^2-y^2 and $3z^2-1$). Below the surface layer each e_g orbital is populated more than a t_{2g} orbital. This is consistent with what is found for bulk Ni.[28,33] At the surface the xz, yz, and $3z^2-1$ orbitals whose lobes point into the vacuum, and whose projected densities of states therefore become more narrow at the surface, gain charge. The xy and x^2-y^2 orbitals, whose lobes lie in the surface layer, lose charge. There are two competing effects which determine the redistribution of charge among the d orbitals: (i) The self-energy increases for orbitals with lobes pointing into the vacuum—this favors depopulation, and (ii) the bandwidth decreases for orbitals with lobes pointing into the vacuum, this increases the population. We see that the second effect dominates and that the depopulation is much more pronounced for the x^2-y^2 than for the xy orbital.

For the five-layer film, the numbers in parentheses were obtained with only the muffin-tin part of the self-consistent potential [see Figs. 3(a)(2) and

TABLE II. Layer- and orbital-projected valence charges.

		Q_{sp}	Q_d	Q_{xy}	$Q_{xz}=Q_{yz}$	$Q_{x^2-y^2}$	$Q_{3z^2-r^2}$
Ni_1		0.62	8.29	1.62	1.70	1.40	1.87
Ni_3	S	0.76	8.34	1.60	1.67	1.65	1.75
	$S-1$	0.92	8.32	1.65	1.60	1.74	1.73
Ni_5	S	0.76	8.32	1.60(1.60)	1.67(1.66)	1.64(1.63)	1.74(1.76)
	$S-1$	0.92	8.34	1.64(1.64)	1.62(1.63)	1.73(1.74)	1.73(1.73)
	$S-2$	0.93	8.34	1.64(1.65)	1.62(1.63)	1.74(1.74)	1.72(1.73)

3(b)(2)]. These numbers are surprisingly similar to those obtained with the full potential [Fig. 3(a)(1) and 3(b)(1)].

B. Spin densities

Since Ni is a strong ferromagnet, i.e., the majority d band is full, the redistribution of charge among the d orbitals at the surface is directly reflected in the orbital projections of the spin density. These are shown in Table III.

The first column gives the spin moment inside the various muffin-tin spheres. It may be seen that for all the films the moment at the surface is larger than inside the film. This is more pronounced for the thinner films and in the extreme case of a monolayer the moment is $0.95\mu_B$. This is in good agreement with the recent calculation of Noffke and Fritsche[26] who find the spin moment for the Ni monolayer to be $0.90\mu_B$. The second column shows the d-spin moments, which are slightly larger than the total moments because the sp orbitals contribute by a small negative amount. The spin density in the interstitial region and in the vacuum regions is extremely small and negative. Finally, we show in the last four columns of Table III and in Fig. 20 how much each d orbital and layer contributes to the spin moment. In Fig. 20 the results of the 13-layer film are shown too, and the dots indicate the amount of spin moment of t_{2g} and e_g character in bulk Ni. The mechanism behind the redistribution of spin moment at the surface layer between the different orbitals was discussed above in connection with the projected densities of states (Fig. 14) and the redistribution of charge.

The t_{2g} orbital of xy character is seen to gain spin moment while the xz and yz orbitals are losing spin moment as the surface is approached. This change of anisotropy was predicted qualitatively by Fulde *et al.*[37] on the basis of a renormalized-atom calculation. The increased moment of xy character arises from the surface states around $\bar{M}_3$ at the top

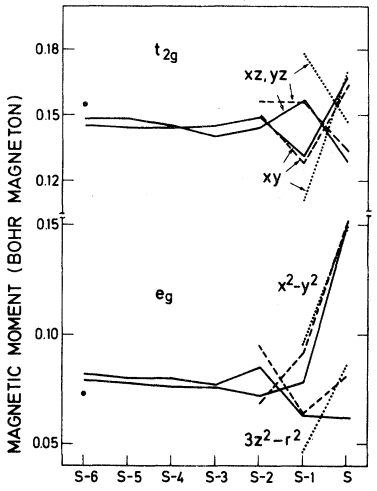

FIG. 20. Variation of the d contributions to the spin magnetic moment (Bohr magnetons per atom) as a function of the layer number measured from the surface (S) for the 13-layer (solid line), the five-layer (dashed line), and the three-layer (dotted line) Ni(001) films. The two dots at the $S-6$ layer indicate the bulk value.

of the spin-up band, i.e., the $\bar{Y}_1$ and $\bar{\Sigma}_2$ states in Fig. 10. The hole at $\bar{M}_3$ slightly reduces the surface moment.

The most important change of moment near the surface is, however, the increase of x^2-y^2 character. This is mainly responsible for the increase of the total moment at the surface. For the monolayer about half the spin moment has x^2-y^2 character. The increased moment results from the surface resonance around $\bar{\Gamma}_4$ at the top of the spin-up band, i.e., the $\bar{\Delta}_2$-$\bar{\Gamma}_4$-$\bar{\Sigma}_1$ band in Fig. 10.

Contours of constant spin density for the five-layer (001) film in the atomic (100) and (001) planes are shown in Figs. 21 and 22. The predominant t_{2g} character of the spin density in the central plane ($S-2$) changes at the surface (S) to nearly cylindrical symmetry due to the increased x^2-y^2 character.

The spin moments for the 13-layer film in Fig.

TABLE III. Layer- and orbital-projected spin moments.

		M	M_d	M_{xy}	$M_{xz}=M_{yz}$	$M_{x^2-y^2}$	$M_{3z^2-r^2}$
Ni_1		0.95	0.95	0.17	0.17	0.42	0.02
Ni_3	S	0.69	0.71	0.17	0.15	0.15	0.09
	$S-1$	0.59	0.61	0.11	0.18	0.09	0.05
Ni_5	S	0.65(0.65)	0.65(0.66)	0.16(0.17)	0.13(0.13)	0.15(0.16)	0.08(0.07)
	$S-1$	0.58(0.59)	0.60(0.62)	0.13(0.14)	0.16(0.16)	0.09(0.09)	0.06(0.07)
	$S-2$	0.61(0.62)	0.63(0.63)	0.15(0.15)	0.16(0.16)	0.07(0.07)	0.09(0.09)

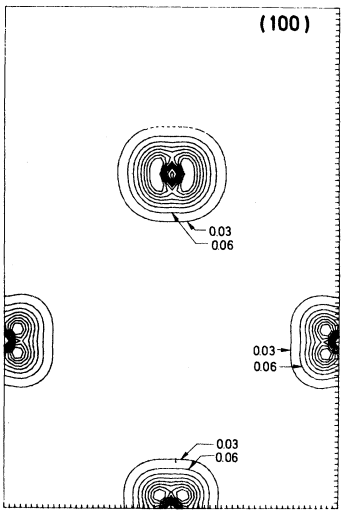

FIG. 21. Contours of constant spin density (μ_B per cubic Bohr radius) on a (100) plane normal to the five-layer film. Density step equals $0.03a_0^{-3}$.

20 were obtained using the muffin-tin part of the five-layer potential as described in Sec. III B. The changes in the d-orbital occupation when the non-muffin-tin part of the potential is ignored is shown

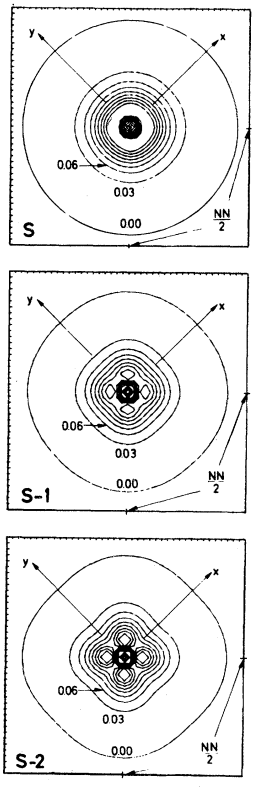

FIG. 22. Contours of constant spin density (μ_B per cubic Bohr radius) for the five-layer film on the atomic plane parallel to the surface. Density step equals $0.03a_0^{-3}$.

in parentheses for the five-layer film in Table III. The insignificant difference between the two calculations justifies the use of the muffin-tin potential in the 13-layer film calculation.

We saw in Figs. 18 and 19 that the densities of states for the three- and five-layer films have more structure close to the Fermi level than the density of states in bulk Ni. One might therefore fear that the exchange splitting obtained from a self-consistent spin-polarized calculation for a five-layer film differs from that of the bulk and, as a consequence, that the calculated magnetic moments are not representative of a semi-infinite Ni crystal. The fine structure in the film density of states could in particular give rise to several stable solutions with different moments. We shall now use LSD Stoner theory[29] to show that this is not the case.

In Stoner theory the total magnetic moment is determined by the condition[29]

$$\bar{N}(m)I = L \ , \tag{5.1}$$

where L is the number of atoms in the unit cell, i.e., the number of layers in the film, and $\bar{N}(m)$ is the magnetization divided by the exchange splitting, i.e., the paramagnetic total density of states per spin averaged about the Fermi level over a range corresponding to m spins. I is the effective exchange-interaction parameter which essentially is

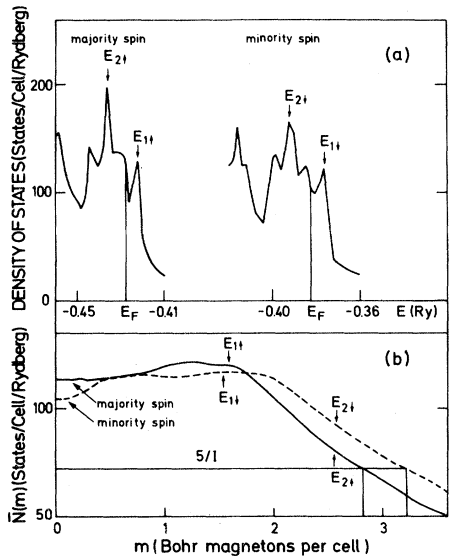

FIG. 23. Construction of the total magnetic moment in the Stoner model for the five-layer Ni film. (a) Unsmoothed total densities of states for the two spin directions and close to the Fermi levels, E_F. (b) Averaged densities of states as function of the magnetic moment.

intra-atomic, such that the value of 69 mRy, found for bulk Ni,[29] may be used here. The solution of Eq. (5.1) written as $\bar{N}(m)=L/I$ is shown in Fig. 23(b) for the five-layer film. Since the paramagnetic density of states is not available we have constructed $\bar{N}(m)$ from the spin-up as well as from the spin-down density of states. These are shown in Fig. 23(a) for the relevant range close to the paramagnetic Fermi enery, which corresponds to an occupancy of 5×5 electrons. The peaks in the densities of states marked E_1 and E_2 are seen to cause very little structure in the averaged densities of states, $\bar{N}(m)$, and can therefore not cause "spurious" solutions.

According to (5.1) the intersection between $\bar{N}(m)$ and the horizontal line at $5/I=72.5$ Ry^{-1} gives the estimated magnetic moment, which is $5\times0.56\mu_B$ for the majority-spin $\bar{N}$ curve and $5\times0.64\mu_B$ for the minority-spin $\bar{N}$ curve. The mean value agrees exactly with the calculated value of $5\times0.60\mu_B$. Figure 23(b) shows that there is only *one* stable solution. A similar construction for the three-layer film gives $3\times0.62\mu_B$ and $3\times0.72\mu_B$, as compared with the calculated value of $3\times0.64\mu_B$. The values for the monolayer are $0.92\mu_B$ and $1.07\mu_B$, as compared with the calculated value of $0.96\mu_B$.

The band contribution to the hyperfine field, or rather to the contact spin density at the Ni nuclei, is negative in the subsurface layers like in bulk Ni,[2] but at the surface we find that the band contribution changes sign and becomes positive. This sign change occurs in both three- and five-layer films.

The contact spin density may be expressed as

$$m(r=0)=n_{s\uparrow}\phi^2_{s\uparrow}(\bar{E}_{s\uparrow},r=0) - n_{s\downarrow}\phi^2_{s\downarrow}(\bar{E}_{s\downarrow},r=0)\ , \tag{5.2}$$

where $n_{s\sigma}$ is the number of s electrons with spin σ in the muffin-tin sphere, and $\phi_{s\sigma}(\bar{E}_{s\sigma},r)$ is the normalized solution of the radial Schrödinger equation. $\bar{E}_{s\sigma}$ is the center of gravity of the occupied part of the $s\sigma$ band, i.e.,

$$\int^{E_F}(E-\bar{E}_{s\sigma})N_{s\sigma}(E)dE=0\ . \tag{5.3}$$

Now, $n_{s\downarrow}$ is larger than $n_{s\uparrow}$ because the exchange splitting of the s band is negligible and the hole in the s band, caused by hybridization with the d band, is full for the up spins but only partially full for the down spins. In the bulk and in the subsurface layers $n_{s\uparrow}-n_{s\downarrow}$ is sufficiently negative that $m(r=0)$ is negative. At the surface, however,

$$n_{s\uparrow}-n_{s\downarrow}=0.226\,04-0.226\,14$$

is still negative but numerically small because the d-band width, and thereby the hybridization hole, is smaller at the surface. Here, the difference between the spin-up and spin-down wave functions becomes important. In order to explain this difference we first recall that $\phi(E,r=0)$ increases with energy because ϕ is normalized in the sphere. If the spin-up and spin-down s electrons had felt the same potential then

$$\phi_{s\uparrow}(\bar{E}_{s\uparrow},r=0)<\phi_{s\downarrow}(\bar{E}_{s\downarrow},r=0)$$

because $\bar{E}_{s\uparrow}<\bar{E}_{s\downarrow}$. The spin-up potential is, however, lower than the spin-down potential and $\phi_{s\uparrow}$ is therefore effectively evaluated at a higher energy than $\phi_{s\downarrow}$. At the surface of the five-layer film we find that $\phi^2_{s\uparrow}(\bar{E}_{\uparrow})=16.37a_0^{-3}$ and $\phi^2_{s\downarrow}(\bar{E}_{\downarrow})16.30a_0^{-3}$ and, hence, a positive contact spin density. For the monolayer $n_{s\uparrow}>n_{s\downarrow}$ and in this case the s-spin moment and the contact-spin density are both positive.

Our $4s$ contribution to the hyperfine field in the central layer of the five-layer film is somewhat smaller than the value of -28 kG calculated for bulk Ni by Wang and Callaway.[2] This difference could be due to our small film thickness or to the relativistic effects included in our calculation. The $4s$ contribution to the hyperfine field calculated for the five-layer film is -17 kG for an atom in the central layer and 8 kG for an atom in the surface layer. If we include a fixed -30 kG contribution from the core as calculated by Wang and Callaway, values of -47 and -22 kG are obtained for the central and surface atoms, respectively. If, on the other hand, we assume that the core contribution scales with the $4s$-spin density at the nucleus values of -35 and $+17$ kG for, respectively, the central and surface atoms are obtained. We thus expect the hyperfine field at the surface to be smaller than, or even of opposite sign to, that in the bulk.

C. Comparison with other calculations

The slight enhancement of the surface magnetic moment that we find from the self-consistent LAPW calculations for the three- and five-layer films disagree with the result of the nine-layer LCAO calculation of Wang and Freeman.[17] These authors find spin magnetic moments of 0.44, 0.58, 0.62, 0.56, and $0.54\mu_B$ when proceeding from the surface to the subsequent layers. Wang and Freeman thus find a substantial reduction of the magnetic moment at the surface and a strongly oscilla-

tory behavior throughout the film. The authors argue that the reduction of the moment at the surface is mainly due to the unoccupied hole pocket in the $\bar{Y}_1$-$\bar{M}_3$-$\bar{\Sigma}_2$ majority-spin surface band. This hole pocket is also present in our energy bands (Figs. 6, 8, and 10) but it is much too small to account for such a large reduction of moment. For the k-space integrations Wang and Freeman (and we also) used the linear triangular method.[21] The energy bands in Ref. 17, and in our Fig. 8, show that of the points in the k mesh only the $\bar{M}$ point is unoccupied and therefore only a fraction of a triangle contributed to the hole. The maximum possible size of the hole therefore corresponds to the area of one full triangle which for the k mesh of 15 points in the irreducible 2D BZ used by Wang and Freeman amounts of $0.06\mu_B$, and this is several times smaller than their quoted moment reduction ($0.58-0.44\mu_B$).

D. Comparison with experiments

Our calculated work functions shown in Table IV are in good agreement with the experimental value[9] for the "semi-infinite" crystal. This holds for all the films considered, except for the monolayer where a somewhat larger value was found.

Since the first suggestion of magnetically dead surface layers on Ni,[13] there have been several attempts to measure the surface magnetic moment. The anomalous Hall-effect measurements on thin Ni films deposited onto nonmagnetic substrates[16] and polarized neutron scattering from fine Ni particles covered with NiO (Ref. 34) both show a few nonmagnetic layers but they are not directly comparable with results for a free surface or an unsupported thin film. The spin polarization of field-emitted[14] and photo-emitted[8,35] electrons from Ni(001) shows a surface magnetic moment similar to the bulk value, however, the accuracy of these measurements is not yet sufficient to determine changes as small as we find.

The spin polarization of electrons extracted from the Ni(001) surface by 150-keV deuteron ions scattered at grazing incidences has been measured.[36] For a reflection angle of 0.2°, which corresponds to a closest contact of about 2 Å, the electron spin polarization is -65%. This large negative polarization seems to indicate that the captured electrons come from close to the Fermi level and this would imply that no dead layers or layers with reversed magnetization exist.

TABLE IV. Calculated work functions (eV) for the various Ni(100) films compared with the experimental value of Ref. 9.

Ni_{13}	Ni_5	Ni_3	Ni_1	Experiment
5.35	5.35	5.29	5.73	5.2

VI. CONCLUSION

In the present paper we have primarily been concerned with the question of how the magnetic moment in a Ni crystal at $T=0$ K is modified near a free (001) surface. Our approach has been within the density-functional formalism to perform self-consistent, spin-polarized band-structure calculations for a series of thin films consisting of one, three, and five atomic layers and then to extrapolate to the semi-infinite crystal.

Great care has been taken in solving the self-consistent-field problem: (1) The LAPW basis functions used form a complete set for any potential which is spherically symmetric inside touching MT spheres and which only depends on $r_\perp$ in the vacuum. This ensures that each LAPW function has the proper radial behavior in the atoms and decays properly into the vacuum. (2) The anisotropy of the potential inside the MT spheres and the corrugation in the vacuum have been treated approximately. (3) A fine mesh has been used in the two-dimensional Brillouin zone, and (4) a large number of iterations have been performed in order to ensure that the spin densities are self-consistent within $0.005\mu_B$ per atom.

An important result, illustrated in Fig. 20 and Table III, is that the behavior of the spin density near the surface is rather similar for one-, three-, and five-layer films, and this makes the extrapolation to the semi-infinite crystal quite safe. We thus expect that the spin moment at the (001) surface of a Ni crystal is enhanced over the bulk value by roughly 10% to about $0.63\mu_B$ per atom and that the enhancement is mostly of $e_g(x^2-y^2)$ character and, to a smaller extent, of $t_{2g}(xy)$ character. The essential mechanism behind this is the narrowing at the surface of the $3z^2-1$, xz, and yz bands and the broadening of the x^2-y^2 and xy bands seen in Fig. 14. The number of d electrons is the same at bulk and surface atoms. We find that the modification of the spin moment is essentially restricted to the surface layer. Moreover, compared with the hyperfine field at a nucleus in the bulk, the hyperfine field at a nucleus at the surface will have a smaller negative, or even a pos-

itive, value.

We have assumed that the distance between the surface and the next layer is as in the bulk. If in reality the surface layer is relaxed outwards by a few percent as LEED measurements might indicate we expect that the enhancement of the moment and the reduction of the hyperfine field will be somewhat larger than estimated above. The largest source of error in our calculations, apart from the LSD approximation, is presumably that the potential set up by the anisotropy of the 3*d* shell is inaccurately represented. We have not attempted a more accurate calculation because it would be very costly, because of known shortcomings of the LSD approximation,[38] and because even the neglect of the large non-MT terms *included* in our self-consistent potential (Fig. 3) did barely influence the results (Tables II and III). Experimental verification or disproval of our predictions should be possible in the near future.

Results of our calculations that may be compared with existing measurements include the work function and the surface bands of small binding energies (0.1 eV) observed in angular-resolved photoemission experiments. The work function agrees with the experimental one to within 0.2 eV (Table IV) but, in order that the surface bands at $\bar{\Sigma}$ and the exchange splitting agree with the experimental results within 0.1 eV, it is necessary to infer a band narrowing due to additional correlation effects as suggested by Liebsch. With this correction also the sign reversal of the electron-spin polarization near threshold can be understood as explained by Pendry. An observed surface band of $\bar{\Delta}_1$ symmetry does not exist in our calculation. While a five-layer film suffices for the calculation of the spin density near a Ni surface, the calculation of surface bands to an accuracy of 0.1 eV (given the LSD approximation) requires a far thicker film. We have peformed a non-self-consistent calculation for a 13-layer film using the MT part of the potential calculated self-consistently for the five-layer film. Apart from the MT approximation this approach is accurate but tedious and a similar treatment of the semi-infinite crystal might have been more appropriate.

ACKNOWLEDGMENTS

We have benefited from discussions with A. Liebsch and J. W. Wilkins. Support from the Danish Natural Science Research Council is gratefully acknowledged.

---

*Present address.

[1]H. Dannan, R. Heer, and A. J. P. Meyer, J. Appl. Phys. 39, 669 (1968).

[2]C. S. Wang and J. Callaway, Phys. Rev. B 15, 298 (1977); The results for the von Barth-Hedin potential have been quoted; V. L. Moruzzi, J. F. Janak, and A. R. Williams, *Calculated Electronic Properties of Metals* (New York, Pergamon, 1978); U. K. Poulsen, J. Kollár, and O. K. Andersen, J. Phys. F 6, L241 (1976); O. K. Andersen, J. Madsen, U. K. Poulsen, O. Jepsen, and J. Kollár, Physics 86-88B, 249 (1977); D. Glötzel and O. K. Andersen, Adv. Phys. (in press).

[3]D. E. Eastman, F. J. Himpsel, and J. A. Knapp, Phys. Rev. Lett. 40, 1514 (1978); F. J. Himpsel, J. A. Knapp, and D. E. Eastman, Phys. Rev. B 19, 2919 (1979); D. E. Eastman and F. J. Himpsel, *Physics of Transition Metals, 1980,* edited by P. Rhodes (Institute of Physics, London, 1981), p. 115.

[4]W. Eberhardt and E. W. Plummer, Phys. Rev. B 21, 3245 (1980).

[5]J. B. Pendry and J. F. L. Hopkinson, J. Phys. F 8, 1009 (1978).

[6]A. Liebsch, Phys. Rev. Lett. 43, 1431 (1979). Also, A. M. Olés and G. Stollhoff (unpublished).

[7]E. P. Wohlfarth, Phys. Lett. 36A, 131 (1971); Phys. Rev. Lett. 38, 524 (1977).

[8]U. Banninger, G. Busch, M. Campagna, and H. C. Siegmann, Phys. Rev. Lett. 25, 585 (1970).

[9]W. Eib and S. F. Alvarado, Phys. Rev. Lett. 37, 444 (1976).

[10]D. G. Dempsey and L. Kleinman, Phys. Rev. Lett. 39, 1297 (1977); D. G. Dempsey, W. R. Grise, and L. Kleinman, Phys. Rev. B 18, 1270 (1978); 18, 1550 (1978).

[11]I. D. Moore and J. E. Pendry, J. Phys. C 11, 4615 (1978).

[12]U. Gradman, J. Appl. Phys. 3, 161 (1974).

[13]L. Lieberman, J. Clinton, D. M. Edwards, and J. Mathon, Phys. Rev. Lett. 25, 232 (1970).

[14]M. Landolt and M. Campagna, Phys. Rev. Lett. 38, 663 (1977).

[15]D. T. Pierce and H. C. Siegmann, Phys. Rev. B 9, 4035 (1974).

[16]G. Bergmann, Phys. Rev. Lett. 41, 264 (1978); Physics Today 32 (8), 25 (1979).

[17]C. S. Wang and A. J. Freeman, J. Appl. Phys. 50, 1940 (1979); Phys. Rev. B 19, 793 (1979); 21, 4585 (1980); J. Magn. Magn. Mater. 15-18, 869 (1980).

[18]Preliminary, not fully converged, results were reported in O. Jepsen, J. Madsen, and O. K. Andersen, J.

Magn. Magn. Mater. 15-18, 867 (1980).
[19]E. W. Plummer and W. Eberhardt, Phys. Rev. B 20, 1444 (1979); J. L. Erskine, Phys. Rev. Lett. 45, 1446 (1980); (private communication).
[20]See AIP documents no. PAPS PRMD-26-2790-10 for 10 pages of the self-consistent potential for the five-layer Ni(001) film. Order by PAPS number and journal reference from American Institute of Physics, Physics Auxiliary Publication Service, 335 East 45th Street, New York, N.Y. 10017. The price is $1.50 for each microfiche, or $5.00 for a photocopy. Airmail additional. Make checks payable to the American Institute of Physics.
[21]O. Jepsen, J. Madsen, and O. K. Andersen, Phys. Rev. B 18, 605 (1978); O. K. Andersen, *ibid.* 12, 3060 (1975).
[22]U. von Barth and L. Hedin, J. Phys. C 5, 1629 (1972).
[23]A. V. MacRae, Science 139, 379 (1963).
[24]J. E. Demuth, P. M. Marcus, and D. W. Jepsen, Phys. Rev. B 11, 1460 (1975).
[25]B. R. Cooper, Phys. Rev. Lett. 30, 1316 (1973); J. Vac. Sci. Technol. 10, 713 (1973); N. Kar and P. Soven, Phys. Rev. B 11, 3761 (1975); B. R. Cooper, *ibid.* 16, 5595 (1977); G. S. Painter, *ibid.* 18, 955 (1978); C. S. Wang and A. J. Freeman, *ibid.* 18, 1714 (1978); F. J. Arlinghouse, J. G. Gay, and J. R. Smith, *ibid.* 20, 1332 (1979), and Ref. 21.
[26]J. Noffke and L. Fritsche, J. Phys. C 14, 89 (1981).
[27]O. K. Andersen, W. Klose, and H. Nohl, Phys. Rev. B 17, 1209 (1978).
[28]O. K. Andersen and O. Jepsen, Physica 91B, 317 (1977).
[29]O. K. Andersen, J. Madsen, U. K. Poulsen, O. Jepsen, and J. Kollár, Physica 86-88B, 249 (1977); O. Gunnarsson, J. Phys. F 6, 587 (1976).
[30]S. L. Weng and M. El-Batanouny, Phys. Rev. Lett. 44, 612 (1980).
[31]W. Eberhardt, E. W. Plummer, K. Horn, and J. Erskine, Phys. Rev. Lett. 45, 273 (1980).
[32]F. J. Arlinghouse, J. G. Gay, and J. R. Smith, Phys. Rev. B 21, 2055 (1980).
[33]L. Hodges, H. Ehrenreich, and N. D. Lang, Phys. Rev. 152, 505 (1966).
[34]M. Sato and K. Hirakawa, J. Phys. Soc. Jpn. 39, 1467 (1975).
[35]S. F. Alvardo, Z. Phys. B 33, 51 (1979).
[36]S. Eichner, C. Rau, and R. Sizemann, J. Magn. Magn. Mater. 6, 204 (1977); C. Rau, Comments Solid State Phys. 9, 177 (1980); C. Rau and S. Eichner, Phys. Rev. Lett. 47, 939 (1981).
[37]P. Fulde, A. Luther, and R. E. Watson, Phys. Rev. B 8, 440 (1973).
[38]O. Gunnarsson and R. O. Jones, J. Chem. Phys. 72, 5357 (1980).